CORE
Metadata, citation and similar papers at core.ac.uk
Provided by HKU Scholars Hub

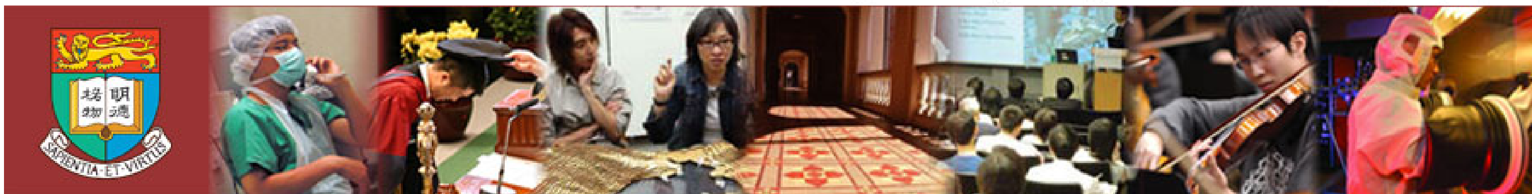

Title	Mechanism of optical degradation in microstructured InGaN light-emitting diodes
Author(s)	Li, ZL; Li, KH; Choi, HW
Citation	Journal Of Applied Physics, 2010, v. 108 n. 11
Issued Date	2010
URL	http://hdl.handle.net/10722/143460
Rights	Journal of Applied Physics. Copyright © American Institute of Physics.

Mechanism of optical degradation in microstructured InGaN light-emitting diodes

Z. L. Li, K. H. Li, and H. W. Choi[a)]
Semiconductor Lighting and Display Laboratory, The University of Hong Kong, Hong Kong

(Received 18 June 2010; accepted 22 October 2010; published online 10 December 2010)

While the enhancement of light extraction efficiency from microstructured InGaN light-emitting diodes (μLED) has been firmly established, there is concern over the effect of microstructuring on the device lifetimes. A study on the electrical characteristics and reliability of μLED arrays has been carried out. Despite improved optical performance, expanded device sidewalls served to accelerate the rate of optical degradation, adversely affect the lifetimes of devices. Through current-voltage plots and noise spectrum measurements, vertical current conduction along the plasma-damaged sidewalls was identified as the key degradation mechanism. © *2010 American Institute of Physics*.
[doi:10.1063/1.3517829]

I. INTRODUCTION

The external quantum efficiency of light-emitting diodes (LEDs) is determined by two main factors: its internal quantum efficiency which is material-dependent, and light extraction efficiency which is determined by design of the device. In order to bridge the gap between the potential of LEDs and the capabilities of present-day devices, extensive efforts in optimizing material growth and device design have been made. Microstructured light-emitting diodes (μLED), consisting of interconnected arrays of micrometer scale light-emitting pixels, have been demonstrated as a feasible method to enhance light extraction by providing additional photon escape pathways through sidewalls of microstructures.[1,2]

The proven advantage of μLEDs over large-area LEDs is its distinctively higher optical output. Photons can be extracted from the sidewalls of the multiple micrometer-scale elements, resulting in reduced re-absorption (and thus heat generation). Many studies on the effects of dimensions and geometry (microdisks,[1] microrings,[3] and microhexagons[4] for instance) have been reported. While the benefits of enhanced light extraction are firmly established, there inevitably will be concerns over the reliability of μLEDs as LEDs are expected to be light sources of exceptionally long lifetime. The formation of a μLED network involves dry etching through the multiquantum wells (MQWs) removing the materials between μLED elements, exposing additional sidewalls. Since the plasma-damaged sidewall terminations are in fact two-dimensional defects, the electrical characteristics and reliability of such devices are potential affected. As a matter of fact, the distinctive geometries of μLEDs facilitate failure analysis of LED devices.

In this paper, the mechanisms of degradation in μLEDs are reported. Interconnected μLEDs of hexagonal and circular geometries are fabricated and characterized, and compared with conventional large area rectangular LEDs. The devices are not passivated after dry etching in order to study the true impact of microstructuring. Device optical spectrum, together with electrical performance, including I-V characteristics, leakage current and noise spectrum are measured. The devices subsequently undergo a 1000 h continuous constant current stress test to determine the optical degradation rate, which is correlated with the device geometries. The effects of vertical conduction along sidewalls on device performance and reliability are discussed.

II. EXPERIMENTAL DETAILS

The structure of the LED wafer used in this study consists of a GaN buffer layer grown on c-plane sapphire substrate, an n-type GaN layer, InGaN/GaN quantum wells, capped with a top contact p-type GaN layer. The emission center wavelength of the wafer is $\sim$465 nm. The LEDs were fabricated using a standard microfabrication process beginning with the deposition of an indium-tin-oxide (ITO) current-spreading layer. The active regions of different geometries were defined by photolithography and dry etched by reactive ion etching using a gas chemistry comprising CHF_3 and Ar to expose the n-contact regions. For μhexagon LEDs, each emissive element is in the shape of a hexagon, with side lengths of 25 μm. These are in turn hexagonally packed into a 12×14 array with a separation of 4 μm. For μdisk LEDs, each emissive element is a disk with a diameter of 50 μm and an array consists of 14×7 interconnected μdisks. The large area LED is of the geometry of a 640×640 μm^2. The effective emissive areas of the large area, μdisk and μhexagon LEDs are 4.1×10^5 μm^2, 3.7×10^5 μm^2, and 4.2×10^5 μm^2, respectively, while their respective sidewall circumferences are 2.88 mm, 18.03 mm, and 21.77 mm. Subsequently, photolithography was carried out again to define the p-pad and p-pad areas. A bi-layer of Ti/Al (50nm/350nm) was deposited as bonding pads, annealed in N_2 at 500 °C for 1 min. The chips were diced by UV nanosecond laser micromachining and packaged into TO headers. Following Al wire-bonding, a silicone encapsulant was applied to protect the device. The optical spectral were measured with an Ocean Optics HR2000 fiber-coupled spectrometer with optical resolution of $\sim$1 nm. The electrical properties, including the I-V characteristics and leakage cur-

[a)]Electronic mail: hwchoi@hku.hk.

 © 2010 American Institute of Physics

Downloaded 28 Nov 2011 to 147.8.21.150. Redistribution subject to AIP license or copyright; see http://jap.aip.org/about/rights_and_permissions

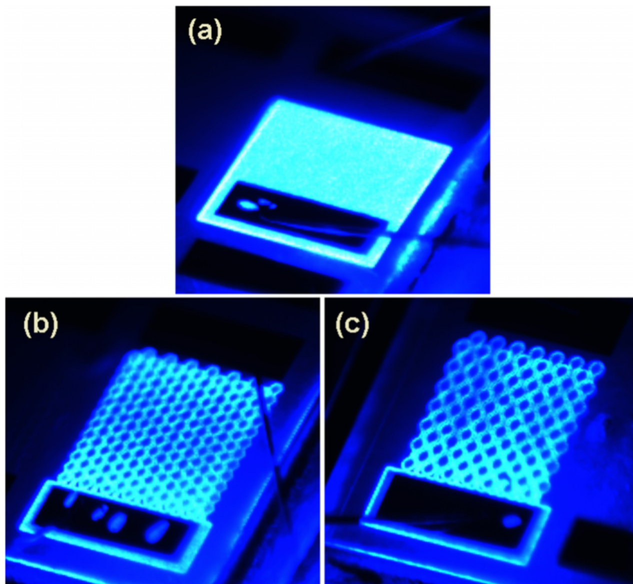

FIG. 1. (Color online) Electroluminescent LEDs of different geometries: (a) large-area; (b) μhexagon array; and (c) μdisk array.

rent of the packaged devices were measured with an HP 4156A precision semiconductor parameter analyzer, while the 1/f noise spectrum was measured by a BTA 9603 FET Noise Analyzer. The devices as shown in Fig. 1, biased at 20 mA, were subsequently subjected to a 900 h continuous stress test at room temperature.

III. RESULTS AND DISCUSSION

Microstructuring of the emission region affects not only the extraction efficiency but also the angular emission characteristics, as a greater component of light is emitted from the sidewalls. As such, the packaged LEDs were placed within a 2 in. integrating sphere to ensure that all the emitted light is collected, while the optical signal was channeled from the output port via fiber to the spectrometer. Figure 2 shows the electroluminescent spectral measured from the devices biased at 20 mA. As noted from the plot, the μLEDs emit 17% more light than the large-area counterpart, attributable to enhanced light extraction from sidewalls of microstructures. Figures 3(a)–3(c) show high-magnification optical microphotographs of the LEDs biased at lower currents to avoid saturation of the charge-coupled device (CCD) camera. Bright edges were observed at the periphery of the microstructures in Figs. 3(b) and 3(c), contributed by laterally propagating photons that have escaped through the sidewalls. These photons contributed to the overall enhancement of light emission. Additionally, a slight spectral blueshift was observed from the μLEDs, which can be attributed to reduced current densities as a result of improved current spreading.

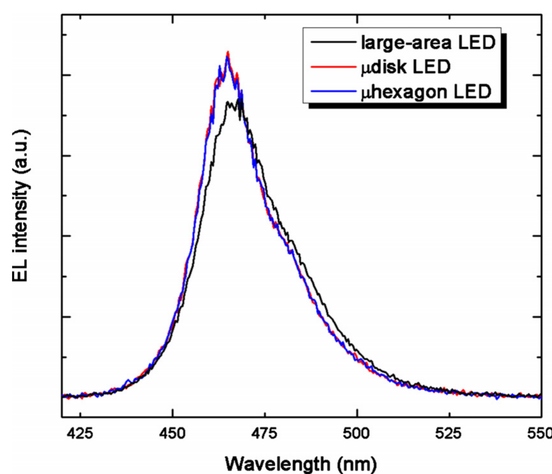

FIG. 2. (Color online) Electroluminescent spectra of the large-area, μhexagon, and μdisk LEDs biased at a current of 20 mA.

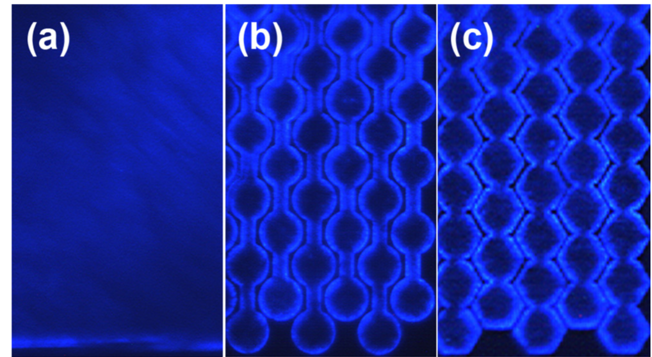

FIG. 3. (Color online) High magnification optical microphotographs showing emission regions of the (a) large-area, (b) μdisk, and (c) μhexagon LEDs.

Insight on device reliability is often provided by its electrical characteristics. The current-voltage (I-V) characteristics of the devices are shown in Fig. 4. The leakage currents of the devices have been extracted from the plots at a reverse bias voltage of 4 V. The magnitude of the leakage current increases from 0.79 mA in large area LED to 3.64 mA in the μhexagon LED and 3.73 mA in the μdisk LED. The slope of the linear region of the I-V curves (in the forward bias region) has also been interpolated to determine the static resistance of the devices. The extracted static resistances are

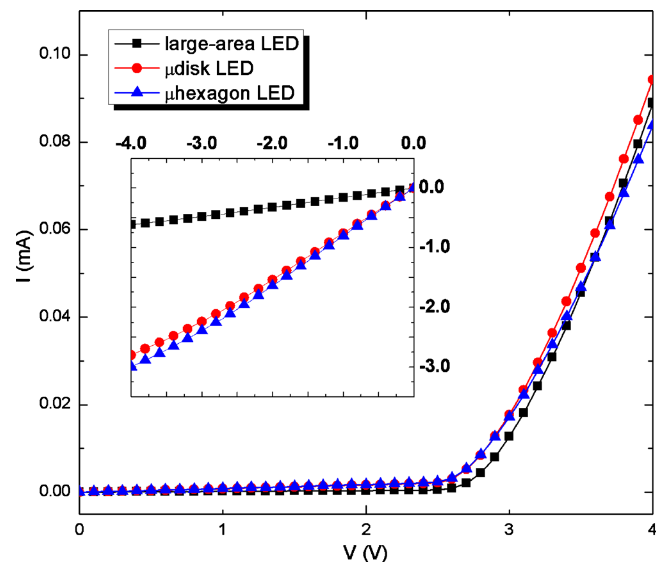

FIG. 4. (Color online) I-V characteristics of the large-area, μhexagon, and μdisk LEDs.

Downloaded 28 Nov 2011 to 147.8.21.150. Redistribution subject to AIP license or copyright; see http://jap.aip.org/about/rights_and_permissions

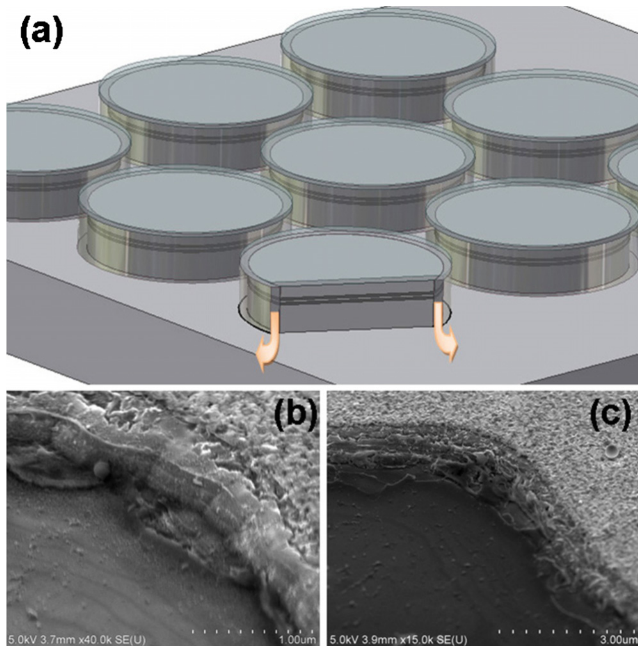

FIG. 5. (Color online) (a) Schematic depicting vertical current flow along sidewalls of μLEDs. Close-up SEM images showing sidewalls of (b) as-etched and (c) stressed devices.

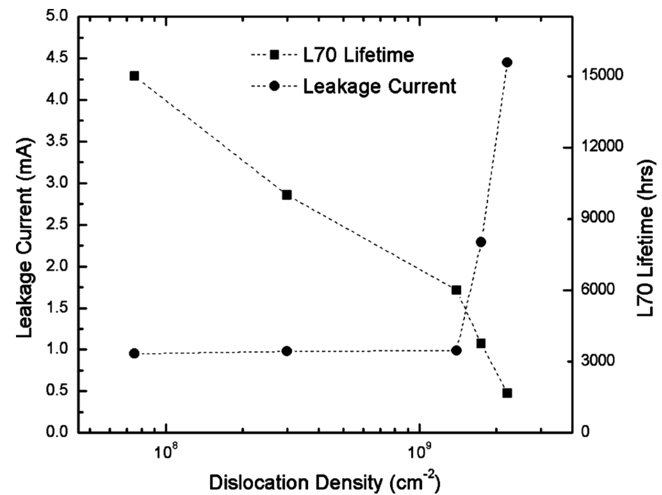

FIG. 6. Plot of reverse leakage currents (at −4 V) and L70 lifetimes as a function of dislocation densities of LEDs.

13.19 Ω, 13.69 Ω, and 13.64 Ω for the large area, μhexagon, and μdisk LEDs, respectively. From these values, it can be seen that microstructuring has a greater effect on current leakage than on forward conduction. As the emission area shrinks, surface effects become more prominent on the electrical properties. In a μLED structure, the MQW active layers are disrupted at the peripheries of individual μLED elements. The exposed sidewall surfaces are highly defective due to the exposure of dangling bonds during plasma etching, whereby the incidence of high energy ions leaves behind crystal damage in the surface regions.[5] Such defects trap carriers and induces carrier scattering, resulting in a higher static resistance and reduced carrier mobility.[6]

Additionally, these interfacial defects may also serve as vertical current conduction pathways in a way similar to that of threading dislocations. During plasma etching, p-type GaN becomes compensated through introduction of shallow donors states,[7] while n-type GaN becomes n+,[6] both of which can be attributed to the formation of nitrogen vacancies as a result of preferential loss of N_2.[8] Consequently, the μLED element can be thought of as being surrounded by a network of defects that are n-type in nature, promoting the vertical conduction of electrons across the p-n junction as illustrated in Fig. 5(a), giving rise to an increase in leakage currents. Vertical conductivity along dislocations had been identified as one of the major causes of breakdown in LEDs,[9] and in p-n junctions in general. In a separate study, the I-V characteristics and lifetimes of a group of LEDs with different dislocation densities (by varying the In concentration in the MQWs) was studied and analyzed, the results of which are summarized in Fig. 6. It was observed that as the dislocation densities of devices increases beyond $\sim 1.5 \times 10^9$ cm^{-2}, the leakage currents (at a reverse bias voltage of 4 V) rises rapidly. On the other hand, the L70 lifetime of devices [L70 lifetime is the time to 70% lumen maintenance, as proposed by ASSIST (Ref. 10)] are drops linearly with increasing dislocation densities. The results positively identify current leakage at sites of dislocations as causes of degradation. Following the same model, the defects generated as a result of microstructuring in μLEDs are expected to play a key role in their enhanced degradation rates.

Another possible contributing factor is the junction curvature effect.[11] The breakdown voltage associated with a spherical junction is significantly reduced compared to a planar junction due to higher field intensities, depending also on the radius of the curvature. The presence of interfacial defects in μLEDs is thus predicted to adversely affect their reliability. The SEM images in Fig. 5(b), showing an as-etched μLED sidewall, and Fig. 5(c), showing the same sidewall after 1000 h operation, further illustrate this point. The sidewall has become significantly rougher with fragmentation due to proliferation of defects. Low-frequency noise measurements were conducted to further study the carrier properties.

Low-frequency noise, especially 1/f noise and generation-recombination (G-R) noise, is sensitively dependent on the presence of defects, traps and dislocations in semiconductors. The noise spectrum accurately reflects the internal material quality and is thus deemed an important tool for determining the reliability of an LED.[12] Figure 7 show plots of the noise spectrum of LEDs with different geometries for frequencies in the range of 3.15 Hz to 16.5 kHz. In an LED (or p-n junction in general) structure, the current spectral density S_I under low current bias can be expressed by the following equation:[13]

$$S_I = \frac{4N_t q I_D}{\tau_r \sigma \nu N_c^2} e^{2E_t/kT}, \tag{1}$$

where N_t is the trap density; a larger N_t generally implies poorer crystal quality, increasing the magnitude of the noise spectrum. τ_r is the recombination time or carrier lifetime, which increases the magnitude of the noise spectrum when the trap density increases, while the other terms have their

Downloaded 28 Nov 2011 to 147.8.21.150. Redistribution subject to AIP license or copyright; see http://jap.aip.org/about/rights_and_permissions

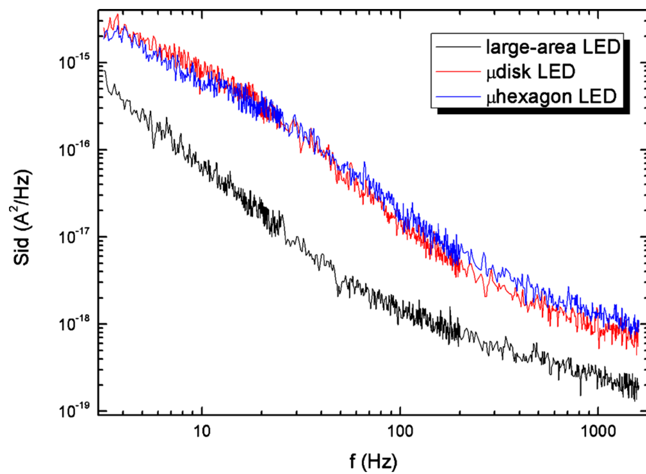

FIG. 7. (Color online) Noise spectrum of LEDs with different geometries.

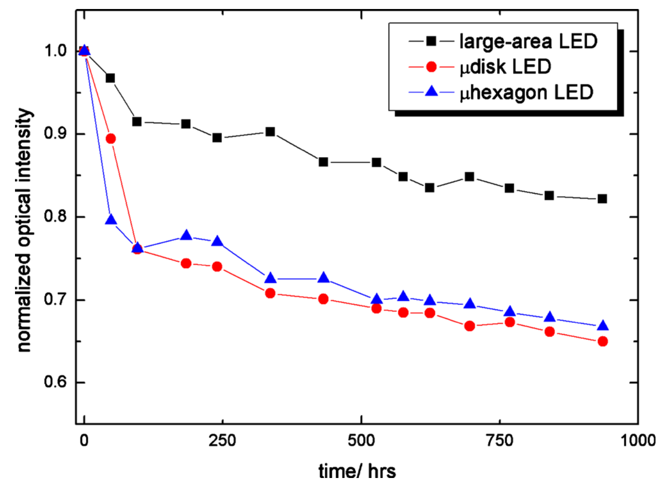

FIG. 8. (Color online) Plot of normalized optical intensity of the large-area, μhexagon, and μdisk LEDs over 1000 h.

usual meanings. From Fig. 7, the noise magnitude for a μLED (irrespective of geometry) is approximately an order of magnitude higher than the corresponding large-area LED. This can be understood from the trapping and de-trapping of carriers along the plasma-damaged sidewalls, whereby the total sidewall areas of the μLEDs were approximately six to eight times larger than the large-area LED. With a higher sidewall ratio, the noise magnitudes of the LEDs are thus significantly enhanced.

The LEDs were then operated for >1000 hrs to determine their rate of degradation. Figure 8 shows the plot of normalized optical intensity over 1000 h, whereby a constant bias current of 20 mA was applied to the devices. While the two large area LEDs maintains ~82% and ~79.5% of their initial optical powers after 900 h, the μdisk LED maintains ~65.5% of its initial optical power, while the μhexagon LED maintains ~67% of its initial optical power. During the 900-h test, the optical output of μLED degraded very quickly during the first 500 h; the degradation rate slows down since then. On the other hand, the large-area LED degraded almost linearly throughout. Assuming linearity, the L70 lifetime for the large-area LED is 2500 h. For the μLEDs, the degradation rate after the initial 100 h of operation becomes linear, and the lifetime $t_{70\%}$ of the μdisk LED and μhexagon LED are found to be ~400 h and ~500 h, respectively. This corresponds to less than 1/5 of the lifetime of a large-area LED. μLEDs, therefore, expected to have shorter lifetimes despite higher extraction efficiency. Expectedly, there is a tradeoff between device performance and reliability. The compromised reliability may be partially alleviated through passivation of sidewalls, control of plasma damage and damage removal, subjects of our on-going studies.

IV. CONCLUSION

In summary, the effects of microstructuring of LEDs have been studied. In terms of optical performance, the increased sidewall surface areas of micro-LEDs certainly promote light extraction efficiency. However, the formation of plasma-damaged sidewalls becomes a threat to the reliability as a result of severe vertical current leakage. A balance should be struck between light extraction and device lifetime.

ACKNOWLEDGMENTS

This work was supported by a GRF grant of the Research Grant Council of Hong Kong (Project No. HKU 7118/09E).

[1] S. X. Jin, J. Li, J. Y. Lin, and H. X. Jiang, Appl. Phys. Lett. **77**, 3236 (2000).
[2] H. W. Choi, C. W. Jeon, M. D. Dawson, P. R. Edwards, R. W. Martin, and S. Tripathy, J. Appl. Phys. **93**, 5978 (2003).
[3] H. W. Choi, C. W. Jeon, and M. D. Dawson, IEEE Photonics Technol. Lett. **16**, 33 (2004).
[4] H. W. Choi and S. J. Chua, J. Vac. Sci. Technol. B **24**, 800 (2006).
[5] H. W. Choi, S. J. Chua, A. Raman, J. S. Pan, and A. T. S. Wee, Appl. Phys. Lett. **77**, 1795 (2000).
[6] S. J. Chua, H. W. Choi, J. Zhang, and P. Li, Phys. Rev. B **64**, 205302 (2001).
[7] X. A. Cao, S. J. Pearton, A. P. Zhang, G. T. Dang, F. Ren, R. J. Shul, L. Zhang, R. Hickman, and J. M. Van Hove, Appl. Phys. Lett. **75**, 2569 (1999).
[8] C. R. Eddy, Jr. and B. Molnar, J. Electron. Mater. **28**, 314 (1999).
[9] B. S. Simpkins, E. T. Yu, P. Waltereit, and J. S. Speck, J. Appl. Phys. **94**, 1448 (2003).
[10] Alliance for Solid-state Illumination and Technologies; website: www.lrc.rpi.edu/programs/solidstate
[11] S. M. Sze and G. Gibbons, Solid-State Electron. **9**, 831 (1966).
[12] F. N. Hooge, T. G. M. Kleinpenning, and L. K. J. Vandamme, Rep. Prog. Phys. **44**, 479 (1981).
[13] S. Sawyer, S. L. Rumyantsev, M. S. Shur, N. Pala, Yu. Bilenko, J. P. Zhang, X. Hu, A. Lunev, J. Deng, and R. Gaska, J. Appl. Phys. **100**, 034504 (2006).

Downloaded 28 Nov 2011 to 147.8.21.150. Redistribution subject to AIP license or copyright; see http://jap.aip.org/about/rights_and_permissions